NRC·CNRC
From Discovery
to Innovation...
De la découverte
à l'innovation...

La Science à l'œuvre pour le
at work for Canada

NRC Publications Archive (NPArC)
Archives des publications du CNRC (NPArC)

A Modeling Approach to the Effect of Resin Characteristics on Parison Formation in Extrusion Blow Molding

Yousefi, Azizeh-Mitra; den Doelder, Jaap; Rainville, Marc-André; Koppi, Kurt A.

Web page / page Web
http://dx.doi.org/10.1002/pen.21251
http://nparc.cisti-icist.nrc-cnrc.gc.ca/npsi/ctrl?action=rtdoc&an=11458021&lang=en
http://nparc.cisti-icist.nrc-cnrc.gc.ca/npsi/ctrl?action=rtdoc&an=11458021&lang=fr

National Research
Council Canada

Conseil national
de recherches Canada

Canada

A Modeling Approach to the Effect of Resin Characteristics on Parison Formation in Extrusion Blow Molding

Azizeh-Mitra Yousefi,[1] Jaap den Doelder,[2] Marc-André Rainville,[1] Kurt A. Koppi[3]
[1] Industrial Materials Institute (IMI), National Research Council of Canada, Boucherville, Quebec, Canada J4B 6Y4

[2] Polyethylene Product Research, Dow Benelux B.V., Terneuzen 4530 AA, The Netherlands

[3] The Dow Chemical Company, 433 Building, Midland, Michigan 48667

The most critical stage in the extrusion blow-molding process is the parison formation, as the dimensions of the blow-molded part are directly related to the parison dimensions. The swelling due to stress relaxation and sagging due to gravity are strongly influenced by the resin characteristics, die geometry, and operating conditions. These factors significantly affect the parison dimensions. This could lead to a considerable amount of time and cost through trial and error experiments to get the desired parison dimensions based upon variations in the resin characteristics, die geometry, and operating conditions. The availability of a modeling technique ensures a more accurate prediction of the entire blow-molding process, as the proper prediction of the parison formation is the input for the remaining process phases. This study considers both the simulated and the experimental effects of various high-density polyethylene resin grades on parison dimensions. The resins were tested using three different sets of die geometries and operating conditions. The target parison length was achieved by adjusting the extrusion time for a preset die gap opening. The finite element software BlowParison® was used to predict the parison formation, taking into account the swell and sag. Good agreements were found between the predicted parison dimensions and the experimental data. POLYM. ENG. SCI., 49:251–263, 2009. Published by Society of Plastics Engineers

INTRODUCTION

The first step in the extrusion blow-molding process is the extrusion of a parison of molten polymer. The extruded parison is then inflated to take on the shape of the surrounding mold and finally the part is cooled and ejected. The shape of the parison, especially its diameter and thickness profiles, strongly affects the final part thickness distribution.

Parison swell and sag are factors that significantly influence the parison dimensions. Parison sag occurs as a result of the parison stretching under its own weight. This thinning effect is more pronounced closer to the die exit [1]. The degree of sag depends on the processing parameters such as melt temperature, suspension time, and total parison length [2], as well as on resin characteristics (e.g., extensional viscosity and damping parameters). Extrudate swell is defined as an increase in the cross-sectional area of the extruded parison. A combination of elongational and shear stresses are applied to the molten polymer as it travels through the die. Once the melt exits the die in the form of a parison, the stress is relieved. As there are no other forces acting on the parison at this point other than its own weight, extrudate swell occurs. The high extrudate swell for molten polymers is a manifestation of the molecular orientation caused by the flow in the die [3]. The extensional stresses associated with stretched polymer chains can be determined by means of birefringence measurements as reported by Brizitsky et al. [4].

The most common representation of the parison swell is in terms of the diameter swell (B_1) and the thickness swell (B_2) defined as

$$B_1 = \frac{D_{\text{parison}}}{D_{\text{die}}}, \qquad (1)$$

$$B_2 = \frac{h_{\text{parison}}}{h_{\text{die}}}, \qquad (2)$$

where D_{parison} and D_{die} are the parison and die diameters, h_{parison} is the parison thickness, and h_{die} is the die gap

opening. The final part thickness distribution is directly related to both diameter swell and thickness swell [5]. Therefore, these two parameters can be combined to define the area swell as follows:

$$B_{\mathrm{area}} = B_1 \times B_2. \qquad (3)$$

One of the earliest techniques for measuring the parison swell is the pinch-off mold, originally proposed by Sheptak and Beyer [6]. Alternative techniques have also been introduced in the literature to measure parison dimensions. DiRaddo and Garcia-Rejon [7] combined the measurements of parison length evolution with time, parison diameter profile, melt flow rate, axial temperature gradient, and a theoretical description of the effects of swell and sag on the parison to estimate the parison thickness and diameter profiles. Perhaps the most accurate method to date has been to extrude the parison into an oil bath having the same temperature and density as the melt and to take photographs of the parison at regular intervals [8]. This method enables the determination of swell as a function of time in the absence of sag. However, because of the complexity of this procedure, the pinch-off mold technique continues to be used.

The extrudate swelling upon emerging from the die is a viscoelastic phenomenon, which can be thought of as a three-step process: a small Newtonian swelling, a sudden elastic recovery, and further swelling due to stress relaxation [9, 10]. For polymer melts, a main contribution to the extrudate swell comes from the memory effect. This is primarily the elastic response to the elongational stresses prevailing at the entrance of the die and, to some extent, to the shear stresses imposed on the melt in the flow channel. With sufficiently long dies the fluid memory fades almost completely, and an asymptotic swelling ratio is reached [10, 11].

In a study on two high-density polyethylene (HDPE) resins taken from successive batches of the same commercial grade, Koopmans [12–14] reported that the maximum swell and the time to reach this value are very sensitive to the molecular weight distribution of the resin. He demonstrated that the flow behavior of polydisperse polymers can be better understood by considering the different molecular weight moments of the resin. Recently, Den Doelder and Koopmans unified experimental swell results in terms of specific combinations of higher moments of the molecular weight distribution of the resin [15]. It is also well established that small variations in the die geometry are usually much more effective in altering the swelling characteristics of an HDPE resin than most of the operating parameters. In light of this, the experimental data collected at a wide range of die geometries, resin characteristics, and operating conditions can be the most efficient technique to validate the finite element simulations and to verify the practical validity of the viscoelastic constitutive equations and the mathematical swell models [14].

In general, the maximum extrudate swell is related to the recoverable strain [13]. The Weissenberg number is a quantity that is mostly used to represent the recoverable strain and is defined as follows [3]:

$$We = \frac{Q\tau}{A_{\mathrm{die}} \; h_{\mathrm{die}}}, \qquad (4)$$

where Q is the volumetric flow rate, A_{die} is the flow channel area at the die exit, and τ is the Maxwell relaxation time represented by the reciprocal of the crossover frequency where the storage modulus (G') and the loss modulus (G'') coincide in dynamic shear tests ($G' = G''$), according to the Maxwell viscoelastic model [14]. The Maxwell relaxation time corresponds to the time associated with an average polymer chain leaving its tube according to the reptation model [16–18].

The main goal of this work is to investigate the effect of resin characteristics on swell and sag. The collected experimental data are compared with the numerical prediction of the parison formation, using the BlowParison® software developed at IMI. This software has been successfully used in the past to model the swell and sag, combined with the nonisothermal effects, for several industrial parts including fuel tanks [19–24]. It is also validated at high Weissenberg numbers ($We > 400$) [25] and extremely high flow rates (>2000 g/s). The software couples a fluid mechanics approach to represent the die flow, with a solid mechanics approach to represent the parison behavior outside the die, and a mathematical swell model to account for the pronounced elongational and shear stresses at high Weissenberg numbers. To our knowledge, this approach is the first that is able to yield stable predictions based on first principles, for high flow rates and small die gap annular systems. The fundamentals of this modeling tool can be found elsewhere [22, 25].

The present work attempts to extend the modeling capabilities of the BlowParison® software to a wider range of resin grades and die geometries. The swell model presented in this work has been improved and validated by over a hundred experimental trials, covering a multitude of die geometries and operating conditions for different HDPE resin grades. Since it is well known that small differences in molecular structure and viscoelastic properties of resins can lead to significant swell differences, it is very important to study the performance of the presented method in relation to how the resin material model input parameters are determined from rheological characterization.

THEORETICAL BACKGROUND

Modeling of Parison Formation

Annular flow occurs in polymer forming operations such as blow-molding and pipe-extrusion processes [26]. The flow of fluids with complex microstructure (e.g.,

molten polymers) cannot be described by classical Navier–Stokes equations. The stresses in such fluids are determined neither by their current state of deformation nor by their current state of motion; instead, the stresses depend on the whole history of the deformation [27]. As a consequence, the numerical simulation of parison formation in extrusion blow molding remains a challenging task when it comes to high production rates, in particular, when high *We* numbers are present.

Many models exist, which are based either on molecular considerations or on modifications of established theories such as linear or nonlinear viscoelasticity [27, 28]. Graham and McLeish [29] made a comparison between the predictions of the "pom-pom" molecular model of McLeish and Larson [30] in exponential shear and the experimental data. Accurate quantitative predictions were reported using the multimode approach and the possibility of using exponential shear to obtain the multimode nonlinear spectrum of a melt was explored. In an extensive review, Crochet and Walters [31] presented the numerical simulation of the flow of highly elastic liquids in complex geometries. The need for suitable constitutive models and stable iterative numerical schemes were emphasized, particularly at high *We* numbers. Yurun and Crochet [32] developed a high-order elastic-viscous split stress/streamline-upwind Petrov–Galerkin finite element method for simulation of steady viscoelastic flows. The method was applied to the flow of a Maxwell fluid around a sphere. Brasseur et al. [33] solved the time-dependent compressible Newtonian extrudate-swell problem with slip at the wall, in an attempt to simulate the stick-slip extrusion instability. It was reported that when the volumetric flow rate at the inlet was in the unstable regime and compressibility was taken into account, self-sustained periodic oscillations of the pressure drop and of the mass flow rate at the exit were observed and the extrudate surface became wavy.

Tanoue and Iemoto [34] calculated the steady-state annular extrudate swell of polymer melts with die gap programming. The Giesekus model was employed as the constitutive equation. The requirement for the unsteady-state calculation when the flow geometry continuously changes was pointed out. The need for experimental trials to validate the simulations was also emphasized. A neural network-based approach was presented by Huang and Liao [35], in which the effects of the die temperature and flow rate on the diameter and thickness swell for HDPE were investigated. A good agreement was reported between experimentally determined parison swell and the predictions, at low flow rates, using the trained neural network model. Gaidai et al. [36] studied the extrudate swell behavior of the IUPAC low-density polyethylene melt and introduced a K-BKZ model [37, 38] with an irreversible Papanastasiou–Scriven–Macosco (PSM) damping function [39]. Faster and more stable solutions at high shear rates were reported compared with similar modeling softwares. More recently, Mitsoulis [40] derived the numerical solu-

tions for the extrudate swell and exit correction in annular flow of pseudoplastic and viscoplastic fluids. Further studies based on the Herschel–Buckley model were proposed to improve the predictions for viscoplastic fluids [41]. An extensive analysis of the existing approaches for the numerical simulation of non-Newtonian and viscoelastic fluids can be found elsewhere [42, 43].

Governing Equations

To calculate the flow stresses for viscoelastic fluids, two different approaches have been used in the scientific literature. In the first approach, the flow kinematics is derived using a generalized Newtonian model, and it is subsequently used as an input for the viscoelastic equation to calculate flow stresses [44]. In the second approach, namely the direct approach, the viscoelastic behavior of the material is taken into account from the beginning to calculate the flow kinematics [45]. Baaijens [45] compared these methods and concluded that there was a good agreement between the two, while the former was more cost effective. That is, the calculation time is significantly reduced upon using the generalized Newtonian model as it does not require the calculation of the whole history of the deformation [27]. The first approach was adopted in the BlowParison® software to predict the stresses experienced by the polymer melt upon the flow in extrusion dies [22, 25]. While the flow kinematics in the die was predicted based on the Hele–Shaw model, assuming Carreau-viscosity-model-type behavior for the melt [46], the particle tracking as well as the deformation prediction was preformed using the K-BKZ viscoelastic model [37, 38, 47].

Flow in the Die. For a fluid obeying the Carreau model, the viscosity takes the following form [46]:

$$\eta = \eta_0 \cdot a_T \left[1 + \left(\lambda \cdot a_T \dot{\gamma} \right)^2 \right]^{\frac{n-1}{2}}. \tag{5}$$

In this equation, η is the viscosity of the polymer melt at the processing temperature, η_0 is the zero-shear Newtonian viscosity at a reference temperature, $\dot{\gamma}$ is the shear rate, n is the power-law index for the shear-thinning zone, λ is a characteristic time representing the transition between the Newtonian and shear-thinning zones, and a_T is the temperature shift factor according to the WLF shift function [48]:

$$\log(a_T) = \frac{-c_1(T - T_{\text{ref}})}{c_2 + (T - T_{\text{ref}})}, \tag{6}$$

where c_1 and c_2 are material parameters, T is the fluid temperature, and T_{ref} is a reference temperature. The Newton–Raphson iterative scheme was used to solve the set of equations for the flow kinematics using the Carreau model [49].

Parison Formation after Exiting the Die. The K-BKZ model is an integral-type viscoelastic model that allows the integration of the deformation history based on the particle tracking technique. The K-BKZ model relates the stress to the strain history as follows [37, 38, 47]:

$$\sigma(t) = -q\delta + \frac{1}{1-\theta}\int_{-\infty}^{t}\sum_{k=1}^{N}[m_k(t-\tau)$$

$$\times\, h_k(I_1,I_2)]\{c^{-1}(\tau,t) + \theta \cdot c(\tau,t)\}d\tau, \quad (7)$$

where q is the hydrostatic pressure, δ is the identity tensor, t is the time, τ is the relaxation time, m is the memory function given by the Maxwell relaxation spectrum, k is the index of the linear-viscoelastic parameter sets for the memory function, N is the total number of the modes, c is the Cauchy deformation tensor, c^{-1} is the Finger deformation tensor, h is the damping function based on the invariants of the Finger tensor (I_1 and I_2), and θ is a parameter that refers to the second normal stress difference in the deformation (biaxial effect). The PSM damping function was used to represent the strain dependency under nonlinear viscoelastic deformation [39, 50]:

$$h_k(I_1,I_2) = \frac{\alpha}{\alpha - 3 + \beta_k I_1(t,\tau) + \{1-\beta_k\}I_2(t,\tau)}, \quad (8)$$

where α and β are the damping coefficients. In this work, a total of six-parameter sets were used for the constitutive model ($N = 6$). The same value of α and β were used for all modes. The thermal dependence of the K-BKZ model was accounted for with the WLF temperature shift function.

The flow kinematics from the Carreau model was used as input to the K-BKZ model so as to calculate the flow stresses developed in the die. The overall stress components evaluated for each element were considered as the initial boundary conditions, knowing that these stresses were being removed at the moment the element emerged from the die. Therefore, the stress relaxation of the semi-solid extrudate was predicted based on the solid-mechanics principles. The distance in the die over which the particle tracking was performed had a pronounced effect on the swell prediction. Upon a wide range of experimental trials, this length was defined in a dimensionless form by the following expression:

$$L_{\text{pt}} = \left(\frac{D_{\text{die}}}{L_{\text{die}}}\right)^{a_1} \cdot [S_1 + a_2 \cdot \ln(De^*)], \quad 0 \le L_{\text{pt}} \le 1. \quad (9)$$

In this equation, a_1 and a_2 are constants, L_{die} is the die length, S_1 is a resin-dependent swell model parameter, and De^* is a modified Deborah number, related to the flow time in the die (t_{f}) and terminal relaxation time of the resin (τ_t) as follows [3]:

$$De^* = \frac{(a_T \cdot \tau_t \cdot a_3)}{t_{\text{f}}}, \quad (10)$$

where

$$\tau_t = \eta_0 \cdot J_s^0 = \eta_0 \frac{\sum_{k=1}^{N}G_k\tau_k^2}{\left(\sum_{k=1}^{N}G_k\tau_k\right)^2}. \quad (11)$$

In *Eqs. 10* and *11*, a_3 is a constant, a_T is the temperature shift factor, J_s^0 is the steady state compliance, and G_k and τ_k are the linear viscoelastic parameter sets for the memory function (relaxation moduli and relaxation times, respectively) given by the generalized Maxwell relaxation spectrum ($N = 6$). The steady-state compliance is a useful property for material characterization. While it is found to be independent of the average molecular weight, it is strongly affected by the molecular weight distribution [3] and could be potentially related to various moments of the molecular weight distribution [51]. At terminal relaxation time, the complete chains have relaxed and therefore the molecular weight and the polydispersity of the polymer are reflected. Thus, in the absence of long-chain branching, it is hypothesized that by incorporating the terminal relaxation time as a parameter in the Hybrid approach, the polydispersity of HDPE grades could be accounted for in the swell prediction.

Effect of the Elongational Forces. The Hybrid fluid mechanics-solid mechanics approach presented in this work is based on the membrane elements for both the flow in the die and parison formation phase, which disregards the three-dimensional nature of the shear flow in the die, particularly at high shear rates. Moreover, the presented numerical formulation does not account for the elongational forces developed at the entrance to the die and in the die land area. To compensate for the negative impact of these hypotheses, the Hybrid approach is coupled with a mathematical swell model. This model makes use of dimensionless quantities ($D_{\text{die}}/L_{\text{die}}$ aspect ratio, Weissenberg and Deborah numbers) to compensate for the elongational forces ignored by the Hybrid approach.

The swell model is developed based on a wide range of experimental trials conducted using different die geometries and operating conditions. This model identifies a recoil factor (RF) and a hoop factor (HF) for each parison programming point, so as to compensate for the underestimated thickness swell and diameter swell, respectively. Therefore, the overall parison swell predicted for each element at each time-step is a combination of the numerically predicted swell and the model-based swell factors,

defined as follows:

$$\mathrm{RF} = C_{\mathrm{R}} \cdot \exp\left[S_2 - (S_2 + a_4) \cdot \left(\frac{We_{\mathrm{u}} - We^*}{We_{\mathrm{u}}}\right)^{a_5}\right], \quad (12)$$

$$\mathrm{HF} = C_{\mathrm{H}} + C_{\mathrm{R}} \cdot \frac{D_{\mathrm{die}}}{L_{\mathrm{die}}} \cdot (1 + De^*). \quad (13)$$

In these equations, a_4, and a_5 are constants, We_{u} is a resin-dependent parameter linearly related to the Maxwell relaxation time of the resin, S_2 is a resin-dependent swell model parameter, and C_{R} and C_{H} are dimensionless die-geometry dependent and resin-dependent parameters, respectively, taking the following forms:

$$C_{\mathrm{R}} = a_6 + (1 - a_6) \cdot \left(\frac{\phi_{\mathrm{m}} - \phi_{\mathrm{b}}}{45}\right), \quad (14)$$

$$C_{\mathrm{H}} = \ln\left(\frac{\tau}{\tau_{\mathrm{ref}}}\right), \quad (15)$$

where a_6 and τ_{ref} are constants, ϕ_{m} and ϕ_{b} are the mandrel and bushing angles, respectively, and τ is the Maxwell relaxation time at the processing temperature. Similar to De^* (Eq. 10), the modified We number (We^*) in Eq. 12 is defined as follows:

$$We^* = \frac{Q \cdot (a_T \cdot \tau_t \cdot a_3)}{A_{\mathrm{die}} h_{\mathrm{die}}}. \quad (16)$$

It should be mentioned that all the constants declared in these equations are material independent.

EXPERIMENTAL

Materials

Five commercial linear HDPE blow-molding resins, coming from three different resin manufacturers, were employed in this study. The resins, denoted A to E, were tested either on a lab-scale or on an industrial-scale extruder using three different sets of die geometries and operating conditions, leading to a wide range of We^* and De^* numbers. Table 1 gives the die geometries considered in these studies. The target parison length was achieved by adjusting the extrusion time for a die gap opening of 1 mm. Prior to experimental trials, all resins were rheologically characterized to obtain the material parameters for the K-BKZ model and for the swell model.

Rheological Characterizations

Linear Viscoelastic Parameters. Dynamic mechanical spectroscopy (DMS) frequency sweep measurements were conducted on the molten resins on a TA Instruments

TABLE 1. Die geometries examined in this work.

Die	D_{b} (mm)	D_{m} (mm)	L_{die} (mm)	L_{dl} (mm)	φ_{b} (°)	φ_{m} (°)
(I)	10.0	8.0	25.0	—	0.0	0.0
(II)	40.0	38.0	41.0	6.0	0.0	45.0
(III)	40.0	38.0	41.0	6.0	30.0	45.0

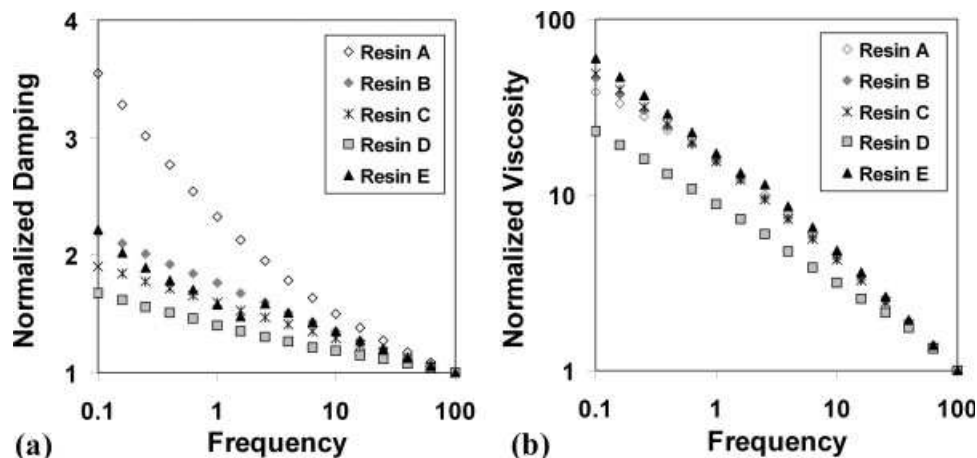The scale bar shows the die gap profile (in mm).

FIG. 1. (a) Normalized damping curve and (b) normalized complex viscosity curve as function of frequency for the resins A to E, obtained using a DMS parallel-plate rheometer.

ARES rheometer with a parallel plate setup. The 25-mm-diameter disk samples were stamped from compression-molded plaques prepared according to ASTM D 1928. The measurements were conducted at three different melt temperatures, covering the processing temperatures used for the experimental parison formation trials. For each sample, frequency sweeps were made from 10^{-1} to 10^2 rad/s at a strain of 10% (linear regime) under an inert nitrogen atmosphere. The storage and loss moduli (G' and G'') and complex viscosity (η^*) curves were obtained as function of frequency. The relaxation times and moduli for the Maxwell relaxation spectrum ($N = 6$) were estimated using the UMat® software developed at IMI. The normalized damping curves were also constructed by dividing the G''/G' values at each frequency to the respective value at the highest frequency (10^2 rad/s). The same procedure was used to construct the normalized complex viscosity curves. Figure 1a and b gives the normalized damping and normalized complex viscosity curves for all the resins, respectively. The zero-shear Newtonian viscosity (η_0), Maxwell relaxation time, and terminal relaxation time at the processing temperature (τ and $a_T \cdot \tau_t$) for these resins are listed in Table 2. For the resin D, the relatively greater shift of the normalized viscosity curve (Fig. 1b) could be an indication of a higher molecular weight distribution. This could also

explain a higher terminal relaxation time estimated for this resin (Table 2).

Nonlinear Viscoelastic Parameters (Damping Function). To determine the strain-dependent part of the K-BKZ model in shear, stress relaxation experiments after a step-strain were performed on a true-shear sliding-plate rheometer (Interlaken). Only the resins D and E were characterized using this technique at 190°C by imposing shear strains ranging from 0.05 to 10. The PSM damping coefficient α was calculated using the following equation [39]:

$$h(I_1, I_2) = \left(\frac{\alpha}{\alpha + \gamma^2} \right), \qquad (17)$$

where γ is the imposed shear strain. Figure 2a shows typical stress relaxation curves at different shear strains. The damping function curve (h vs. γ) for the resin E is given in Fig. 2b, where the estimated α is displayed.

To provide an estimation of the damping coefficient α in the absence of step-shear data, a linear correlation was developed at IMI between the estimated α for the resins D and E, and the area under their respective normalized damping curves from DMS measurements (see Fig. 1a). Subsequently, for the resins A to C, the value of α was approximated using the developed correlation. The damping parameter α for all the resins is listed in Table 2. The effect of damping coefficient β was identified to be non-significant in the Hybrid approach for the presented case studies. This was inferred by running a set of sensitivity analyses using the BlowParison® software, in an effort to investigate the effect of this parameter on final parison dimensions (results not presented). As a consequence, a default value of $\beta = 0.1$ was used in the present work.

Swell Model Parameters. For the resins A and C, the observed experimental parison length of 230 mm in the

TABLE 2. Zero-shear Newtonian viscosity (η_0), damping coefficient α, ultimate We number (We_u), and Maxwell and terminal relaxation times at the processing temperature (τ and $a_T \cdot \tau_t$) for the HDPE resins.

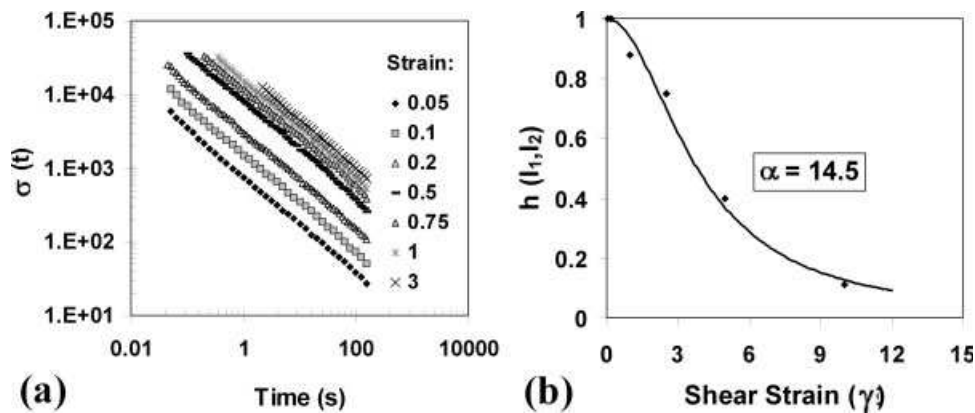| Resin	η_0 (MPa s)	α	We_u	τ (s)	$a_T \cdot \tau_t$ (s)
A	0.13	9.0	320	0.6	34
B	0.18	13.5	275	1.5	43
C	0.23	15.0	173	3.5	42
D	0.14	22.0	312	0.8	54
E	0.26	14.5	155	3.9	39

FIG. 2. (a) Typical stress relaxation curves at 190°C, measured at different shear strain values; (b) corresponding damping function curve for the resin E where the estimated damping coefficient α is displayed.

trial "a" was targeted by inverse modeling, through adjusting the swell parameter S_1 (Eq. 9). As these experiments were conducted at extremely low flow rates, the contribution of the swell model component of the Hybrid approach would reduce to Eq. 9. In other words, the effects of RF and HF (Eqs. 12 and 13) would disappear at very low flow rates. Therefore, the simulation of parison formation could be used to estimate the swell parameter S_1. Knowing that a significant decay of the normalized damping curve as a function of frequency represents a more dominant loss modulus at high temperatures, a correlation was developed at IMI to relate the approximated S_1 values for these resins to the slope of their respective DMS damping curves (Fig. 1a). The higher the slope is, a more pronounced sagging and a less significant swelling is expected for the resin, leading to a reduced value for the swell parameter S_1. This correlation was validated and fine-tuned by comparing the experimental and simulated parison lengths, at low flow rates, for over 10 other HDPE grades from different resin manufacturers (results not shown). The following equation was found to closely provide the swell parameter S_1 for the HDPE grades:

$$S_1 = p_1 \cdot \ln(n_d) + p_2, \tag{18}$$

where p_1 and p_2 are the correlation parameters, and n_d is the absolute value of the slope calculated for the normalized damping curve.

In a similar manner, a correlation was created for the swell parameter S_2 (Eq. 12) by inverse modeling, through a comparison between a high number of experimentally observed parison dimensions and the numerical predictions at high flow rates. It was found that for HDPE grades, this parameter was related to the damping parameter α as follows:

$$S_2 = p_3 \cdot \exp(p_4 \cdot \alpha), \tag{19}$$

where p_3 and p_4 are the correlation parameters. For the resins A to E, the estimated swell parameters S_1 and S_2,

along with the Maxwell and terminal relaxation times, are graphically presented in Fig. 3.

Parison Formation Trials

Lab-Scale Extruder. In the trial "a" (Table 3), the experiments were conducted at Dow Benelux B.V. on resins A to C, using a lab-scale extruder with annular die setup at a die gap of 1 mm, outer die diameter of 10 mm, and mass flow rate of 0.15 g/s. This corresponds to an apparent shear rate of 41.9 s^{-1}. Diameter swell was measured from high-resolution photographs at a distance of 50 mm from the die exit, at the moment of first passage after cutting the strand at the exit. Thickness swell at the same position was calculated from a mass balance and from velocity determined from successive photographs. In addition, the weight swell was determined from weighing the samples once the target parison length of 230 mm was achieved, and dividing the values by the calculated weight of a parison featuring the same length, without swell and sag. Table 3 gives the operating condition for this series of experiments.

Industrial-Scale Extruder. The experiments were conducted at IMI on the resins D and E, using an intermittent extruder from Placo equipped with a pinch-off mold. Two different diverging dies, featuring different bushing angles, were used in this study (trials "b" and "c," Table 3). The preliminary tests conducted to determine the flow rate evolution revealed that there was a time delay of 15–20 s, depending on the accumulator ejection speed, before a steady flow rate was achieved. In light of this, to provide a steady flow rate prior to the pinch-off mold closing, the parison was allowed to extrude for 20 s and was then manually cut off with a pair of scissors. It should be noted that in a real industrial process, bottles would be produced during start-up as the machine lined out to a steady operation. If such bottles were defect in any way, they would most likely be recycled back into the opera-
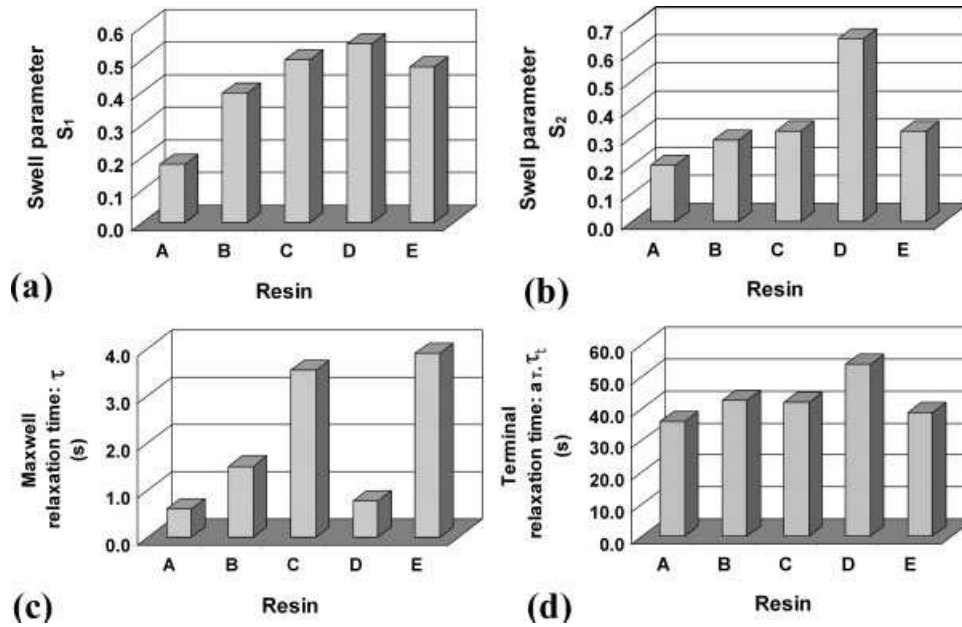
FIG. 3. Estimated material parameters for the resins A to E; (a) swell model parameter S_1; (b) swell model parameter S_2; (c) Maxwell relaxation time τ; (d) terminal relaxation time $a_T \cdot \tau_t$.

tion. Moreover, to account for the variable flow rate in intermittent extrusion, the experimental flow rate evolution profile can be used as input data to the software for numerical simulations [25]. However, to simplify the data analysis, the start-up period was excluded in this study.

The parison produced after this start-up period was used for swell measurements. When the target parison length was achieved, the pinch-off mold was closed and formed a series of cushions along the length of the parison. The pinched-off parison was allowed to cool for 48 h before the measurements were taken. The parison was then cut up into their individual cushions and each cushion was weighed and their width and length were recorded. The diameter and thickness swell for each cushion were determined in the following manner, using *Eqs. 1* and *2*:

$$D_{\text{parison}} = \frac{2L}{\pi} f, \qquad (20)$$

$$h_{\text{parison}} = \frac{w}{2Lh\rho_s} f, \qquad (21)$$

where

$$f = \left(\frac{\rho_s}{\rho_m} \right)^{\frac{1}{3}} \qquad (22)$$

is a function that accounts for the shrinkage, ρ_s and ρ_m are the solid and melt densities, respectively, L is the cushion width, h is the cushion height, and w is the cushion weight. The weight swell for each cushion was also estimated as follows:

$$B_w = \frac{w}{w_0}, \qquad (23)$$

$$w_0 = \frac{\pi}{4} \left[D_b^2 - (D_b - 2h_{\text{die}})^2 \right] \cdot hf\rho_s. \qquad (24)$$

In these equations, D_b is the bushing diameter, and w_0 is the cushion weight without swell and sag. It is shown in a previous study that the weight swell from pinch-off mold, or from the dissected final part, can efficiently represent the combined effect of the diameter and thickness swell, in the same manner as the area swell [25]. In light of this, in the present study the overall parison swell is presented either in terms of the diameter and thickness swell or in terms of the weight swell.

During the experimental trial "b" (Table 3), the resins D and E were extruded through a die gap of 1 mm at a steady flow rate of 10 g/s to achieve the target length of 230 mm. The diverging die used for these experiments had a bushing angle of $0°$ causing a significant variation in the die gap within the die land area, leading to a high contraction in this zone (die II, Table 1). It is shown that this configuration could cause a significant thickness swell for the extruded parison [25].

TABLE 3. Operating conditions used for the parison formation trials: (a) lab-scale extruder; (b, c) industrial-scale extruder.

Trial	Resin	Die	T_{melt} (°C)	Flow rate (g/s)	Die gap (mm)	Parison length (mm)	
						Exp.	Sim.
a	A, B, C	I	190	0.15	1	230	216, 212, 233
b	D, E	II	200	10	1	230	210, 231
c	D	III	200	30	1	230	225

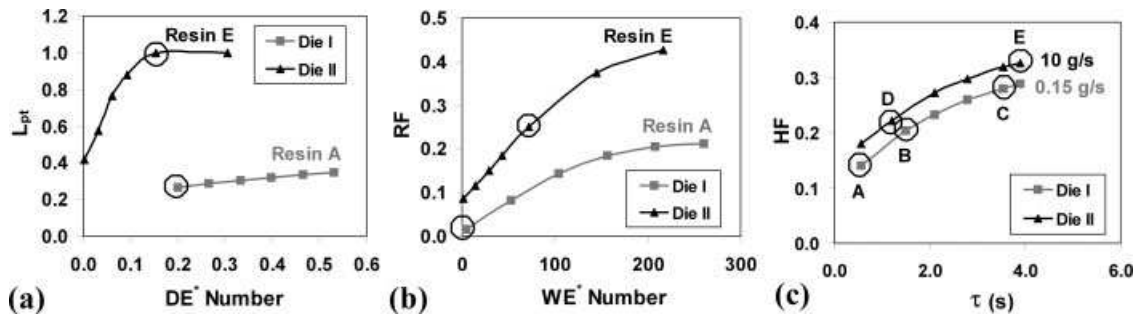The experimental and predicted parison lengths are also compared.

FIG. 4. Swell model variables estimated for the dies I and II; (a) dimensionless distance used in the particle tracking for the resins A and E as a function of De^* number (different flow rates); (b) recoil factor for the resins A and E as a function of We^* number (different flow rates); (c) hoop factor at the flow rate of 0.15 and 10 g/s as a function of Maxwell relaxation time. The circles identify the active values for the resins (trials "a" and "b").

To reduce the effect of die land contraction on the thickness swell, a new die with a bushing angle of 30° was designed at IMI (die III, Table 1). The trial "c" was performed using this die geometry, where the resin D was extruded at a die gap of 1 mm to achieve the target length of 230 mm. The weight swell profile and the extrusion time to achieve the target parison length were compared with the ones obtained in the trial "b".

NUMERICAL SIMULATIONS

IMI's BlowParison® software was used to predict the parison formation, taking into account the swell and sag, as well as the nonisothermal effects. In the simulations, a three-node membrane element was used to create the finite element mesh of the parison (40,000 to 70,000 elements depending on the parison length).

RESULTS AND DISCISSION

Characteristics of the Swell Model

Figure 4a and b give the swell model variables estimated for the dies I and II using the resins A and E,

respectively (trials "a" and "b"). The dimensionless distance used in the particle tracking (L_{pt}) for the dies I and II as a function of De^* number, calculated at different flow rates, is presented in Fig. 4a. The circles identify the active values of L_{pt} (0.26 and 1.0) at the operating conditions used in these trials. The lower value of L_{pt} for the resin A is quite expected as this resin was extruded at an extremely low flow rate (0.15 g/s). Moreover, this resin had a lower terminal relaxation time (Table 2), leading to a lower value of L_{pt}. Figure 4b presents the RF for the two dies as a function of We^* number, calculated at different flow rates. The circled RF values (0.02 and 0.25 for the resins A and E, respectively) imply that the elongational forces are significantly higher for the die II (trial "b"). This is primarily attributed to the higher contraction in the die land zone for this die. In Fig. 4c, the HF is plotted as a function of Maxwell relaxation time for the two dies (I and II) at their respective flow rates (0.15 and 10 g/s). The values identified in this figure correspond to the active HF values for the resins A to E (trials "a" and "b"). Because of the higher value of HF for the resin E, a higher sudden elastic swelling is expected for this resin after exiting the die. It should be mentioned that the very low swell factors (RF and HF) estimated for the trial "a"
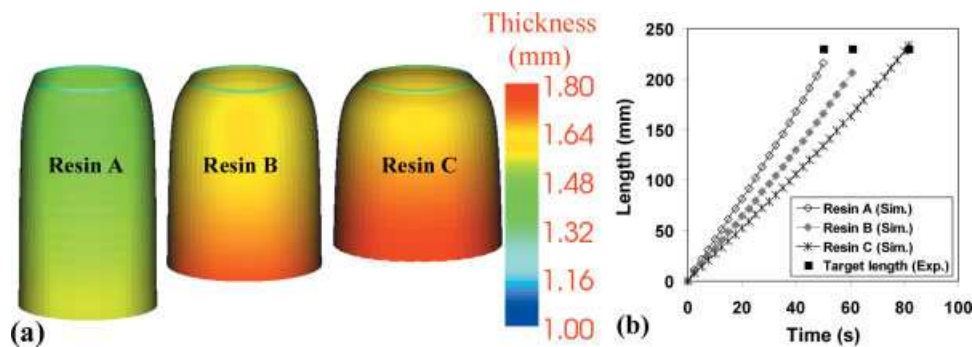

FIG. 5. (a) Simulated parison swell for the resins A, B, and C after 5 s of extrusion on the lab-scale extruder (gap = 1 mm, flow rate = 0.15 g/s); (b) predicted parison length evolution as a function of time for the three resins. The solid squares indicate the experimental length at their respective extrusion times. [Color figure can be viewed in the online issue, which is available at www.interscience.wiley.com.]
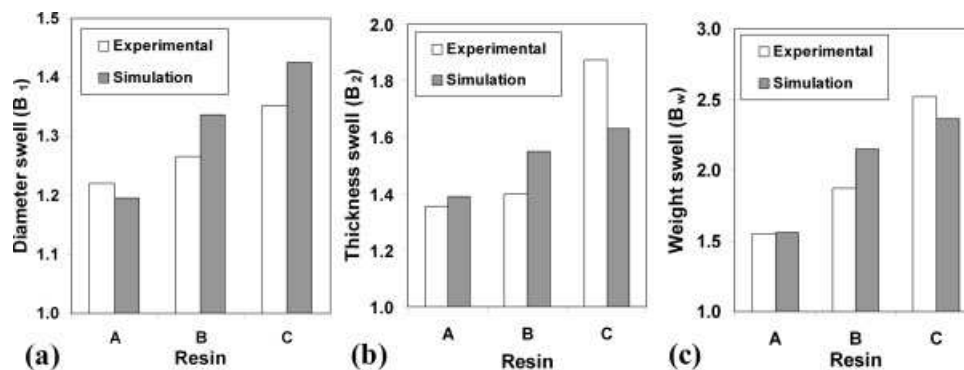
FIG. 6. Comparison between the experimental and simulated parison dimensions for the resins A to C, at 50 mm below the die exist (gap = 1 mm, flow rate = 0.15 g/s); (a) diameter swell; (b) thickness swell; (c) weight swell for the final parison (length = 230 mm).

indicate that the swell prediction for this experiment has a negligible dependence to the swell factors (RF and HF). Therefore, the swell prediction is performed primarily by the solid-mechanics component of the Hybrid approach, almost independent from the swell model.

Comparison Between Experimental and Simulated Parison Dimensions

Lab-Scale Extruder. For the resins A to C, Fig. 5a shows the simulated parison swell after 5 s of extrusion at a flow rate of 0.15 g/s. It can be seen that the resin A has a much lower diameter swell, mainly because of its lower Maxwell relaxation time. The thickness swell gradually increases toward the bottom of the parison because of the time-dependent stress relaxation and viscoelastic swelling, governed by the K-BKZ relaxation spectrum. The predicted parison length evolutions as function of time are presented in Fig. 5b. The solid square symbols identify the experimental parison length for the three resins (230 mm) at the given extrusion times. The simulated parison lengths, listed in Table 3, show up to 10% error in all cases. To some extent, the observed discrepancy could be attributed to the uncertainty in the damping coefficient α for these resins.

In Fig. 6a and b, the diameter and thickness swell measured at 50 mm below the die exit are compared with the corresponding simulation results. The experimental and simulated weight swell values for the final parison are compared in Fig. 6c. Both the diameter and thickness swell show their lowest value for the resin A and have their highest value for the resin C. Even if the simulated diameter and thickness swell are either overestimated or underestimated (up to 10%), the order of swelling is correctly predicted in all cases. Hence the final weight swell predictions are in good agreement with the experimental data. Based on these results, the BlowParison® software is able to predict the swelling characteristics of these three resins with an acceptable accuracy. These results show that the numerical method used here is capable of

discriminating between resins that have significantly different viscoelasticity. Future work will focus on the potential of the method to predict and resolve swell differences between resins that have a similar rheological signature. This will also provide more insight into the validity of some assumptions taken here to relate viscoelastic data to input parameters for the model.

Industrial-Scale Extruder. Figure 7a shows the simulated parison swell for the resins D and E at the end of extrusion at a die gap of 1 mm (die II, trial "b"). The diameter swell is considerably higher for the resin E because of its higher elasticity (higher Maxwell relaxation time). In Fig. 7b, the predicted diameter and thickness swell profiles for the resin D are compared with the experimental data. For this resin, both predicted swell profiles are in good agreement with the experimental data. As for the resin E (Fig. 7c), the thickness swell is under-predicted close to the die exit. The predicted diameter swell, however, is fairly good showing only a slight over-
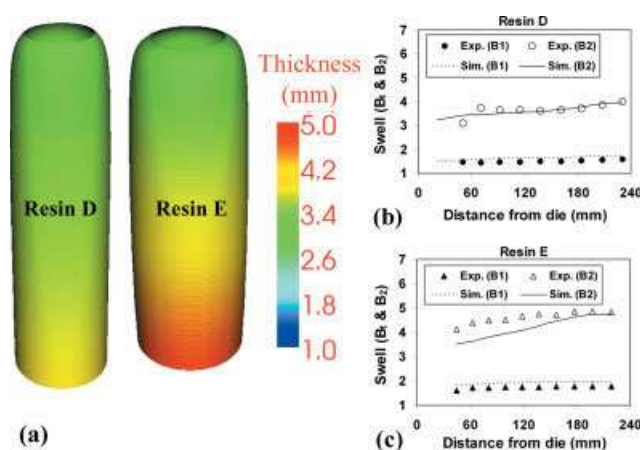

FIG. 7. (a) Simulated parison swell for the resins D and E at the end of extrusion using the die II (gap = 1 mm, flow rate = 10 g/s); (b) comparison between the experimental and predicted diameter and thickness swell for the resin D; (c) corresponding results for the resin E. [Color figure can be viewed in the online issue, which is available at www.interscience.wiley.com.]
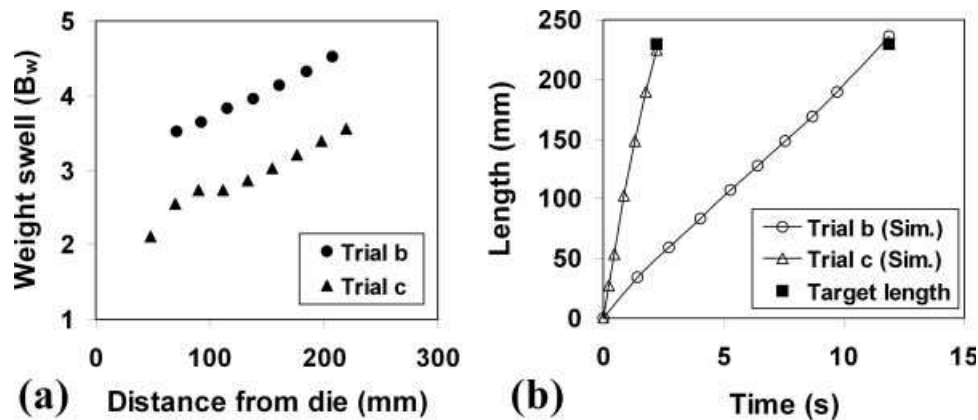
FIG. 8.   (a) Comparison between the experimental weight swell profiles for the resin D using the dies II and III; (b) predicted parison length evolutions as function of time. The solid squares represent the experimental length at their respective extrusion times.

prediction for this high-swelling resin. Comparing these results to the corresponding data in the trial "a" (Figs. 5 and 6), the thickness swell is significantly higher in the trial "b" mainly because of the specific geometry of the die II, featuring a high difference between the bushing and mandrel die angles [25]. See also *Eqs. 12–14*, suggesting increased elongational forces for this die geometry.

For the trial "c," the experimental weight swell profile along the parison extruded through the die III is presented in Fig. 8a. To compare the extent of swell caused by the two dies (II and III), the corresponding experimental weight swell data from the trial "b" are also plotted in this figure. Even if the flow rate was three times higher in the trial "c," the weight swell is considerably reduced

in this trial, using the die III, because of the reduced elongational forces in the die land area. These results also prove that small variations in the die geometry are much more effective in altering the swelling characteristics of HDPE resins than the operating conditions [12–14]. For both dies, the predicted parison length evolutions as function of extrusion time are given in Fig. 8b. The solid squares identify the target experimental length at their respective extrusion times. It can be seen that at a given extrusion time, the die III leads to a much longer parison as a result of the reduced weight swell, which is not proportional to the increased flow rate. The predicted parison lengths are in a very good agreement with the experimental data (Table 3).
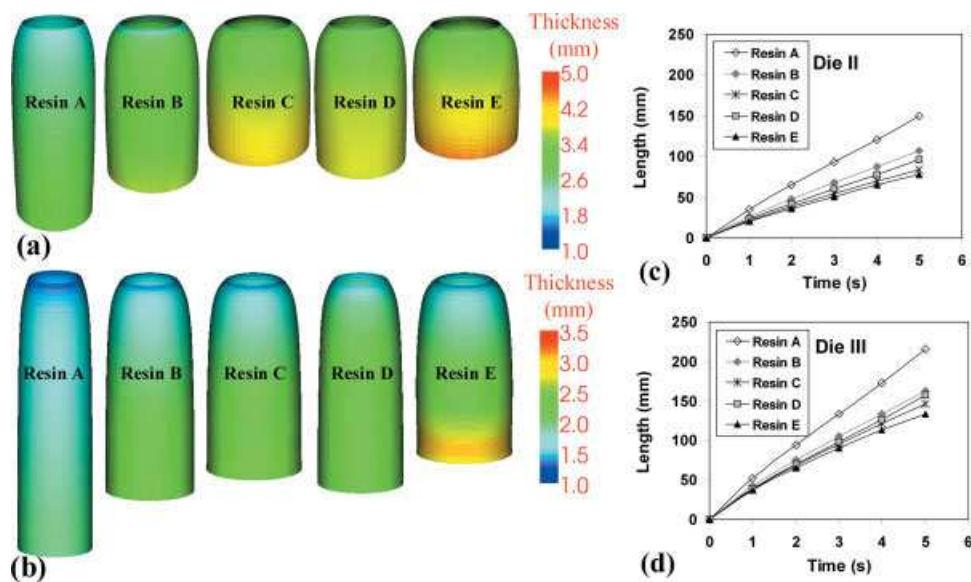

FIG. 9.   (a, b) Simulated parison swell for all the resins after 5 s of extrusion using the die II and III, respectively; (c, d) predicted parison length evolutions as function of time using the two dies, respectively (gap = 1 mm, flow rate = 10 g/s). [Color figure can be viewed in the online issue, which is available at www.interscience.wiley.com.]

Reducing the Resin and Part Design Times by Modeling

The current practice for designing new parts could be quite time consuming because of the complex nature of the swell and sag characteristics for the blow-molding resins. A modeling tool that could predict the parison dimensions upon any variations in the resin characteristics, die geometry, die gap programming, and operating conditions could significantly reduce the resin and part design times and costs. In an effort to demonstrate this capability, the predicted parison dimensions for all the five resins using the dies II and III are compared in Fig. 9a and b. The corresponding parison length evolutions are presented in Fig. 9c and d. Knowing that the simulation results for the resin D are validated by the experimental data (trials "b" and "c"), and the order of swell for these resins have been confirmed throughout the experimental validations in this study, the presented results could be considered as being reliable enough for design purposes. In other words, for a resin featuring a significant swelling, appropriate die geometry could be proposed by modeling. The same argument holds if one desires to choose a resin for an existing die geometry and a desired cycle time. More validation data on the successful use of the presented modeling tool for a multitude of complex industrial parts can be found elsewhere [24].

CONCLUSION

This work presented the strong dependence of parison dimensions on resin characteristics and die geometry. IMI's BlowParison® software was used to predict the parison formation, taking into account the swell and sag. The comparison between the predicted parison dimensions and experimental data demonstrated the capability of this modeling tool in predicting the parison length and swell profiles. Therefore, the parison dimensions from simulation could be readily used as the starting point for process design, reducing the resin and part design times and costs. This work also demonstrated that a modeling approach capable of creating the link between the rheological properties of the resin and parison swell and sag could be the key to a better material design and a better control over the thickness distribution for the final part. Future work will focus on the potential of the presented approach to predict swell differences between resins that have a similar rheological signature. This will also provide more insight into the validity of some assumptions taken here to relate viscoelastic data to the input parameters for the Hybrid approach.

REFERENCES

1. A. Midgley and E.A. Peszel, *SPE ANTEC Tech. Pap.*, 1131 (2002).

2. N. Orbey and J.M. Dealy, *Polym. Eng. Sci.*, **24**, 511 (1984).

3. J.M. Dealy and K.F. Wissbrun, *Melt Rheology and Its Role in Plastics Processing*, Van Nostrand Reinhold, New York (1990).

4. V.I. Brizitsky, G.V. Vinogradov, A.I. Isayev, and Y.Y. Podolsky, *J. Appl. Polym. Sci.*, **27**, 751 (1978).

5. R.W. DiRaddo, A. Garcia-Rejon, L. Pecora, and D. Poirier, *SPE ANTEC Tech. Pap.*, 1026 (1994).

6. N. Sheptak and C.E. Beyer, *SPE J.*, **21**, 190 (1965).

7. R.W. DiRaddo and A. Garcia-Rejon, *Polym. Eng. Sci.*, **32**, 1401 (1992).

8. A. Garcia-Rejon and J.M. Dealy, *Polym. Eng. Sci.*, **22**, 158 (1982).

9. D.V. Rosato and D.V. Rosato, *Blow Molding Handbook*, Hanser Publishers, New York (1989).

10. J. Vlachopoulos, *Rev. Def. Beh. Mat.*, **3**, 219 (1981).

11. M.A. Huneault, P.G. Lafleur, and P.J. Carreau, *Polym. Eng. Sci.*, **30**, 1544 (1990).

12. R.J. Koopmans, *Polym. Eng. Sci.*, **32**, 1741 (1992).

13. R.J. Koopmans, *Polym. Eng. Sci.*, **32**, 1750 (1992).

14. R.J. Koopmans, *Polym. Eng. Sci.*, **32**, 1755 (1992).

15. C.F.J. den Doelder and R.J. Koopmans, *J. Non-Newtonian Fluid Mech.*, **152**, 195 (2008).

16. P.G. de Gennes, *J. Chem. Phys.*, **55**, 572 (1971).

17. M. Doi and S.F. Edwards, *The Theory of Polymer Dynamics*, Clarendon Press, Oxford (1986).

18. C.C. Hua and H.Y. Kuo, *J. Polym. Sci. Part B: Polym. Phys.*, **38**, 248 (2000).

19. A.M. Yousefi, P. Collins, and R. DiRaddo, *SPE ANTEC Tech. Pap.*, 864 (2003).

20. A.M. Yousefi, D. Laroche, P. Collins, and R. DiRaddo, *SPE Blow Molding Div. Newslett.* (Spring 2003). Available online: http://www.blowmoldingdivision.org/.

21. A.M. Yousefi, D. Laroche, P. Collins, and R. DiRaddo, Presented at The 6th EsaForm Conference, Salerno, Italy (2003).

22. A.M. Yousefi and H. Atsbha, *Polym. Eng. Sci.* (in press).

23. P. Debergue, D. Laroche, A.M. Yousefi, R. DiRaddo, and H. Atsbha, Presented at *The 24th Annual Meeting of the Polymer Processing Society (PPS-24)*, Salerno, Italy, June 15–19 (2008).

24. F. Thibault, A.M. Yousefi, R.W. DiRaddo, and H. Atsbha, Presented at *The PPS-22 Conference*, Yamagata, Japan (2006).

25. A.M. Yousefi, P. Collins, S. Chang, and R.W. DiRaddo, *Polym. Eng. Sci.*, **47**, 1 (2007).

26. Z. Tadmor and C.G. Gogos, *Principles of Polymer Processing*, SPE Monograph Series, Wiley, New York (1979).

27. M. Renardy, *J. Non-Newtonian Fluid Mech.*, **90**, 243 (2000).

28. M. Renardy, *Ann. Rev. Fluid Mech.*, **21**, 21 (1989).

29. R.S. Graham and T.C.B. McLeish, *J. Rheol.*, **45**, 275 (2001).

30. T.C.B. McLeish and R.G. Larson, *J. Rheol.*, **42**, 81 (1998).

31. M.J. Crochet and K. Walters, *Ann. Rev. Fluid Mech.*, **15**, 241 (1983).

32. F. Yurun and M.J. Crochet, *J. Non-Newtonian Fluid Mech.*, **57**, 283 (1995).

33. E. Brasseur, M.M. Fyrillas, G. Georgios, and M.J. Crochet, *J. Rheol.*, **42**, 549 (1998).

34. S. Tanoue and Y. Iemoto, *Polym. Eng. Sci.*, **39**, 2172 (1999).

35. H.X. Huang and C.M. Liao, *Polym. Test.*, **21**, 745 (2002).

36. O. Gaidai. J. den Doelder, S. de Vries, and A. van de Ven, "Extrudate Swell Analysis and Simulations for the IUPAC-LDPE Melt using the K-BKZ Model," *Technical Report*, Eindhoven University of Technology, The Netherlands (2005).

37. A. Kaye, *College of Aeronautics*, Cransfield, Note No. 134 (1962).

38. B. Bernstein, E. Kearsley, and L.J. Zapas, *Trans. Soc. Rheol.*, **7**, 391 (1963).

39. A.C. Papanastasiou, L.E. Scriven, and C.W. Macosco, *J. Rheol.*, **27**, 387 (1983).

40. E. Mitsoulis, *J. Non-Newtonian Fluid Mech.*, **141**, 138 (2007).

41. E. Mitsoulis, S.S. Abdali, and N.C. Markatos, *Can. J. Chem. Eng.*, **71**, 147 (1993).

42. M.J. Crochet, A.R. Davies, and K. Walters, *Numerical Simulation of Non-Newtonian Flow*, Elsevier, New York (1984).

43. J.A. Brydson, *Flow Properties of Polymer Melts*, George Godwin Ltd., London (1981).

44. L. Douven, *Towards the Computation of Properties of Injection Moulded Products*, Ph.D. Thesis, Technische Universiteit Eindhoven, The Netherlands (1991).

45. F.P.T. Baaijens, *Rheol. Acta*, **30**, 284 (1991).

46. C.L. Tucker III, *Computer Modeling for Polymer Processing—Fundamentals*, Hanser Publishers, New York (1989).

47. D. Laroche, K.K. Kabanemi, L. Pecora, and R.W. DiRaddo, *Polym. Eng. Sci.*, **39**, 1223 (1999).

48. M.L. Williams, R.F. Landel, and J.D. Ferry, *J. Am. Chem. Soc.*, **77**, 3701 (1955).

49. K.K. Kabanemi, J.F. Hetu, and A. Garcia-Rejon, *Int. Polym. Process.*, **12**, 182 (1997).

50. X.L. Luo and R.I. Tanner, *Int. J. Numer. Methods Eng.*, **25**, 9 (1988).

51. M. Kurata, Towards the computation of properties of injection moulded products. *Macromolecules*, **17**, 895 (1984).